Pflugers Arch - Eur J Physiol (2015) 467:1881–1898
DOI 10.1007/s00424-014-1619-7

Localizations of Na^+-D-glucose cotransporters SGLT1 and SGLT2 in human kidney and of SGLT1 in human small intestine, liver, lung, and heart

Ivana Vrhovac · Daniela Balen Eror · Dirk Klessen · Christa Burger · Davorka Breljak · Ognjen Kraus · Nikola Radović · Stipe Jadrijević · Ivan Aleksic · Thorsten Walles · Christoph Sauvant · Ivan Sabolić · Hermann Koepsell

Received: 23 June 2014 / Revised: 16 September 2014 / Accepted: 23 September 2014 / Published online: 11 October 2014

Abstract Novel affinity-purified antibodies against human SGLT1 (hSGLT1) and SGLT2 (hSGLT2) were used to localize hSGLT2 in human kidney and hSGLT1 in human kidney, small intestine, liver, lung, and heart. The renal locations of both transporters largely resembled those in rats and mice; hSGLT2 and SGLT1 were localized to the brush border membrane (BBM) of proximal tubule S1/S2 and S3 segments, respectively. Different to rodents, the renal expression of hSGLT1 was absent in thick ascending limb of Henle (TALH) and macula densa, and the expression of both hSGLTs was sex-independent. In small intestinal enterocytes, hSGLT1 was localized to the BBM and subapical vesicles. Performing double labeling with glucagon-like peptide 1 (GLP-1) or glucose-dependent insulinotropic peptide (GIP), hSGLT1 was localized to GLP-1-secreting L cells and GIP-secreting K cells as has been shown in mice. In liver, hSGLT1 was localized to biliary duct cells as has been shown in rats. In lung, hSGLT1 was localized to alveolar epithelial type 2 cells and to bronchiolar Clara cells. Expression of hSGLT1 in Clara cells was verified by double labeling with the Clara cell secretory protein CC10. Double labeling of human heart with aquaporin 1 immunolocalized the hSGLT1 protein in heart capillaries rather than in previously assumed myocyte sarcolemma. The newly identified locations of hSGLT1 implicate

Ivan Sabolić and Hermann Koepsell, both senior authors, contributed to this study with equal intellectual and organizational input.

Electronic supplementary material The online version of this article (doi:10.1007/s00424-014-1619-7) contains supplementary material, which is available to authorized users.

I. Vrhovac · D. Balen Eror · D. Breljak · I. Sabolić (✉)
Molecular Toxicology Unit, Institute for Medical Research and Occupational Health, Ksaverska cesta 2, 10000 Zagreb, Croatia
e-mail: sabolic@imi.hr

D. Klessen
Institute of Anatomy and Cell Biology, University of Würzburg, Würzburg, Germany

C. Burger
Merck KgaA, Darmstadt, Germany

O. Kraus
Clinical Hospital Sisters of Mercy, Zagreb, Croatia

N. Radović
Clinical Hospital Dubrava, Zagreb, Croatia

S. Jadrijević
Clinical Hospital Merkur, Zagreb, Croatia

I. Aleksic · T. Walles
Department of Thoracic and Cardiovascular Surgery, University Hospital of Würzburg, Würzburg, Germany

C. Sauvant
Department of Anesthesiology and Critical Care Medicine, University Hospital Halle, Halle, Saale, Germany

H. Koepsell (✉)
Department of Molecular Plant Physiology and Biophysics, Julius-von-Sachs-Institute, Institute of Anatomy and Cell Biology, University of Würzburg, Koellikerstr. 6, 97070 Würzburg, Germany
e-mail: Hermann@Koepsell.de

several extra renal functions of this transporter, such as fluid absorption in the lung, energy supply to Clara cells, regulation of enteroendocrine cells secretion, and release of glucose from heart capillaries. These functions may be blocked by reversible SGLT1 inhibitors which are under development.

Keywords Clara cells · Enteroendocrine cells · Human organs · Immunolocalization · mRNA expression · Na^+-D-glucose cotransport · Proximal tubules · Sex differences

Introduction

Transmembrane movements of glucose in mammalian cells are performed by members of the *SLC2* transporter family (glucose transporters or uniporters (GLUTs)) that mediate facilitative diffusion of D-glucose [51] and by members of the *SLC5* family (sodium-glucose cotransporters or symporters (SGLTs)) that mediate cotransport of D-glucose with sodium [56]. The Na^+-D-glucose cotransporters of the *SLC5* family are able to concentrate D-glucose in cells. The best characterized and most strongly expressed SGLT subtypes are SGLT1 (gene *SLC5A1*) and SGLT2 (*SLC5A2*). SGLT1 and SGLT2 differ in sodium-D-glucose stoichiometry, substrate selectivity, sites of expression, and regulation. Several species differences between identical SGLT subtypes have been identified. Thus, human SGLT3 (hSGLT3) is a glucose-gated ion channel, whereas porcine SGLT3 is a Na^+-D-glucose cotransporter [12]. Human SGLT1 (hSGLT1) is upregulated, whereas rabbit SGLT1 is downregulated by stimulation of protein kinase C [56]. In kidney of female rats, higher expressions of SGLT1 (rSglt1) and SGLT2 (rSglt2) were observed compared to male rats [2, 44], whereas an opposite sex difference (males > females) was found for expression of SGLT2 (mSglt2) in the mouse kidney [44]. At variance, no gender dependence was observed concerning the expression levels of SGLT1 in the rat small intestine [2].

The current understanding of physiological functions of SGLT1 and SGLT2 in humans is almost entirely restricted to their role in small intestine and/or kidney [56]. It is based on functional characterizations of the overexpressed human transporters, on pathological phenotypes of patients containing nonfunctional mutants in small intestine and kidney [56], and on characterizations of intestinal and renal phenotypes of mice in which *mSglt1* or *mSglt2* had been removed [16, 53]. Because a detailed immunocytochemical localization of SGLT1 and SGLT2 in human small intestine, kidney, and other organs has not been performed, the functions of these transporters have been discussed assuming that the distributions of these transporters in humans are identical to rodents [56]. Furthermore, it remained unclear whether the expression levels of hSGLT1 and hSGLT2 in kidney are sex-dependent as has been observed in rodents.

Our knowledge concerning the expression of hSGLT1 and hSGLT2 in organs apart from kidney and intestine is almost exclusively based on the analyses of mRNAs. In addition to intestine and kidney, *hSGLT1* mRNA has been detected in heart, testes, prostate, colon, trachea, brain, spinal cord, spleen, lung, liver, uterus, and pancreas [8, 36, 59]. In addition to kidney, *hSGLT2* mRNA has been found in testis, cerebral arteries, and cerebellum [8, 56, 59].

In the present study, we generated polyclonal antibodies against specific peptide sequences of the hSGLT1 and hSGLT2 proteins. After verifying their selectivity and subtype specificity, we investigated the location of hSGLT1 protein in human small intestine and kidney and of hSGLT2 protein in kidney of both sexes. In both organs, hSGLT1 and hSGLT2 proteins showed similar locations but sex-independent expression levels compared to those in rodents, including the presence of hSGLT1 in enteroendocrine K and L cells, as previously shown in mice [16]. To select additional organs for immunocytochemical localization studies, we performed mRNA determinations by reverse transcriptase-polymerase chain reaction (RT-PCR) in liver, lung, heart, adipose tissue, and brains. We detected *hSGLT1* mRNA in liver, lung, and heart and demonstrated hSGLT1 protein in luminal membranes of hepatic duct cells, in alveolar epithelial type 2 cells, bronchiolar Clara cells, and heart capillaries. The findings implicate so far unrecognized physiological and pathophysiological roles of SGLT1 in lung and heart.

Materials and methods

Materials

RNA from human tissues was purchased from Clontech Laboratories, Inc. (Cedarlane, CA). The fluorescence fading retardant Vectashield was purchased from Vector Laboratories Inc. (Burlingame, CA), the molecular weight markers for Western blotting from Bio-Rad (Hercules, CA), methotrexate hydrate (MTX; M8407) from Sigma (St. Louis, MO), and blasticidin (R210-01) from Life Technologies (Darmstadt, Germany). Superfrost/Plus microscope slides were from Thermo Fisher Scientific (USA). All other materials were obtained as described earlier [2, 16, 42, 44].

Antibodies

In these studies, the following primary antibodies were used: Our novel (noncommercial) polyclonal antibodies against amino acids 581-599 (QEGPKETIEIETQVPEKKK-C) of the hSGLT1 protein (hSGLT1-Ab) and against amino acids 591-609 (ESAMEMNEPQAPAPSLFRQ-C) of the hSGLT2 protein (hSGLT2-Ab) were raised in rabbits, as described before for rat antibodies [13, 14]. Generation of polyclonal antibodies against

amino acids 576-595 (EEKSQEETDDGVEEDYPEKS-C) of human SGLT3 (hSGLT3-Ab) and against amino acids 585-600 (PKDTIEIDAEAPQKEK-C) of rat SGLT1 (rSglt1-Ab) has been described earlier [2, 12]. The antibodies were affinity-purified using the respective antigenic peptides coupled via a C-terminal cysteine to polyacrylamide particles using the SulfoLink Kit from Pierce (Bonn, Germany). In addition, in one experiment (Fig. 11 i-k), we used a commercial antibody raised in goat against a peptide of hSGLT1 (hSGLT1-comAb) from Everest Biotech (Oxfordshire, UK; EB09310)). In preliminary experiments using different organs, we observed that the immunostaining efficiency and specificity of hSGLT1-comAb were comparable to that obtained with hSGLT1-Ab and that hSGLT1-comAb immunoreactivity could be blocked with the antigenic peptide EBP09310 supplied by the company (data not shown). Polyclonal antibody to rat water channel aquaporin 1 (AQP1-Ab), which cross-reacts with the human protein, was noncommercial [43]; in heart, AQP1 is expressed in endothelial cells of the microvasculature [40, 41]. Commercial monoclonal antibodies to pan-actin (actin-Ab), α-tubulin (tubulin-Ab), and human Na/K-ATPase α1-subunit (Na/K-ATPase-Ab) were from Merck Millipore (Darmstadt, Germany; MAB1501R), Sigma (St. Louis, MO; T5168), and Santa Cruz Biotechnology (Santa Cruz, CA; sc-48345), respectively. Commercial monoclonal antibody to human lysosomal membrane glycoprotein CD68 (CD68-Ab) was from DakoCytomation (Glostrup, Denmark; M0876); this glycoprotein is highly expressed in macrophages [49]. Commercial polyclonal anti-human Clara cell protein CC10 antibody (CC10-Ab) was from Santa Cruz (sc-9770); the CC10 protein binds surfactant and has anti-inflammatory effects [20, 49]. Polyclonal antibodies against human glucose-dependent insulinotropic peptide (Y-20; sc-23554; GIP-Ab) and glucagon-like peptide 1 (C-17; sc-7782; GLP-1-Ab) were obtained from Santa Cruz.

The following secondary antibodies were purchased commercially: CY3-labeled goat anti-rabbit IgG (GAR-CY3) and donkey anti-goat IgG (DAG-CY3) antibodies, and alkaline phosphatase-labeled goat anti-rabbit IgG (GAR-AP) and goat anti-mouse IgG (GAM-AP) antibodies were from Jackson ImmunoResearch Laboratories (West Grove, PA). Fluorescein isothiocyanate (FITC)-labeled goat anti-rabbit IgG (GAR-FITC) and goat anti-mouse IgG (GAM-FITC) antibodies were from Kirkegaard and Perry (Gaithersburg, MD). FITC-labeled chicken anti-goat IgG (CAG-FITC) and chicken anti-rabbit IgG (CAR-FITC) antibodies were from Santa Cruz. Alexa Fluor 555-labeled goat anti-rabbit IgG (GAR-AF555) and Alexa Fluor 488-labeled chicken anti-goat IgG (CAG-AF488) were purchased from Life Technologies (Darmstadt, Germany).

Preparation of cells stably transfected with hSGLT1, hSGLT2, hSGLT3, or human peptide transporter 1 (hPEPT1)

Baby hamster kidney (BHK)-21 cells were obtained from the American Type Culture Collection (ATCC) company. The cells were stably transfected with hPEPT1 (gene *SLC15A1*, negative control), hSGLT1 (*SLC5A1*), hSGLT2 (*SLC5A2*), or hSGLT3 (*SLC5A4*). Genes were cloned into pCI-neo plasmid (Promega) containing CMV promoter and cotransfected with pCI plasmid which contains dhfr gene at position of neo gene. A ratio of 20:1 (transporter expression plasmid/dhfr coding plasmid) was used for transfections. About 10^7 cells were transfected using the calcium phosphate method (Invitrogen) with 20 μg plasmid DNA. Transfected cells were selected in Dulbecco's modified Eagle's medium (DMEM) containing 10 % inactivated and dialysed FCS, 1 mg/ml G418, and 20–200 nM MTX. Single clones were tested for stable expression of the transporters using gene-specific primers (hPEPT1) and radioactive uptake assays with [^{14}C] α-methyl-D-glucopyranosid (AMG) for SGLT-transfected cells.

Cells were cultivated at 37 °C (10 % CO_2) in DMEM containing 5 % fetal calf serum, 20 nM MTX, and 1 mg/ml G418. For preparation of total cell membranes (TCM) and immunocytochemistry, cells were grown to confluency on Petri dishes, harvested by scraping, collected by centrifugation for 5 min at 1,000×*g*, smeared on glass slides, fixed for 30 min with 4 % *p*-formaldehyde (PFA), rinsed with phosphate-buffered saline (PBS), and further processed in immunocytochemical procedure as described for tissue cryosections (*vide infra*).

Human tissues

The employed procedures for collections and the use of human tissues were approved by the Institutional Ethics Committees in Zagreb (Croatia) and Würzburg (Germany). Informed patient consent was obtained beforehand. Tissue samples from kidneys, jejunum, liver, and abdominal fat were obtained from the hospitals in Zagreb. The samples were obtained from the adult male and female patients that underwent surgical operations to remove tumors or during organ transplantation. Care was taken to collect virtually healthy tissue outside the resected tumors. The patients were between 30 and 47 years old. The female patients had regular menstrual cycles; however, the tissues were collected without considering the cycle stage. Before surgery, the patients did not receive chemotherapy or other anti-tumor treatments. Lung and heart tissues were obtained from the university hospital in Würzburg. Lung tissue (about 1 cm^3) was obtained from the tissue margins of resected lung lobes following routine thoracic surgery. Atrial heart tissue was derived from patients undergoing routine amputation of the left atrial appendage as prophylaxis for postoperative thromboembolic

events. Left ventricular tissue was obtained from patients which underwent myectomy for septal hypertrophy during aortic valve replacement for treatment of aortic stenosis. Immediately following surgical removal, tissue samples were either fixed using 4 % PFA for immunocytochemistry (all organs) or transfered in ice-cold PBS buffer to the laboratory, where it was homogenized and TCM were isolated (kidney and small intestine).

Fixation, freezing, and cryosectioning of tissues

Pieces of the human tissues were fixed for 24 h at 4 °C in PBS containing 4 % PFA. The fixative was removed by four rinses with PBS and one rinse with PBS containing 0.02 % NaN_3 (each rinse 10–15 min). Until use, the tissues were stored refrigerated at 4 °C in PBS containing 0.02 % NaN_3. Before cryosectioning, tissues were incubated overnight with PBS containing 30 % sucrose, embedded in Tissue-TeK (Sakura, Japan), and frozen at −25 °C. Four micrometer-thick cryosections were cut in a Leica CM 1850 cryostat (Leica Instruments, Nussloch, Germany). Sections were collected on Superfrost/Plus microscope slides, dried at room temperature for 2–3 h, and kept refrigerated at 4 °C until further use.

Immunostaining of tissue cryosections

Rehydration of cryosections, antigen retrieval, and incubation steps with the primary and secondary antibodies were described in details before [2]. The optimal antigen retrieval in cryosections of most tissues was achieved by heating in a microwave oven in 10 mM citrate buffer, pH 6, for 20 min, whereas cryosections of the heart tissue were heated in the same buffer for 5 min to obtain optimal staining, other steps being identical to previously described [2].

For single staining with either hSGLT1-Ab, hSGLT2-Ab, or hSGLT3-Ab, the SGLT-transfected cells or tissue cryosections were incubated with the antibody overnight in a refrigerator with PBS containing optimized concentrations of the respective affinity-purified antibody (1:1,000–1:200), followed by rinsing in PBS buffers and incubation for 1 h at room temperature with GAR-CY3, and rinsing in PBS buffers [2].

For double staining with hSGLT1-Ab and hSGLT2-Ab (Fig. 3), cryosections were first incubated overnight in a refrigerator with hSGLT1-Ab, rinsed, incubated for 2 h at room temperature with GAR-FITC, rinsed, incubated overnight in a refrigerator with hSGLT2-Ab, rinsed, incubated for 20 min at room temperature with GAR-CY3, and rinsed in PBS. In other double staining experiments, cryosections were stained with the first primary antibody overnight in a refrigerator, then with the corresponding secondary antibody at room temperature for 1 h, then with the second primary antibody in a refrigerator overnight, followed by the respective secondary antibody at room temperature for 1 h. A care has been taken that the respective pair of primary antibodies was of different kinds (polyclonal vs. monoclonal) or from different hosts (two polyclonal antibodies). Accordingly, the following pairs of primary antibodies were used in these experiments: hSGLT1-Ab/tubulin-Ab, hSGLT1-Ab/CC10-Ab, CC10-Ab/tubulin-Ab, hSGLT1-Ab/CD68-Ab, hSGLT1-Ab/Na/K-ATPase-Ab, hSGLT2-Ab/Na/K-ATPase-Ab, AQP1-Ab/Na/K-ATPase-Ab, and hSGLT1-comAb/AQP1-Ab.

For double staining with GIP-Ab and hSGLT1-Ab or GLP-1-Ab and hSGLT1-Ab, sections were first incubated with GIP-Ab or GLP-1-Ab overnight in a refrigerator, rinsed with PBS buffers, incubated with CAG-AF488 for 1 h at room temperature, rinsed with PBS buffers, incubated with hSGLT1-Ab overnight in a refrigerator, rinsed with PBS, incubated with GAR-AF555 for 1 h at room temperature, and washed. For each tissue, optimal dilution of primary antibodies was defined in preliminary experiments (data not shown), whereas optimal dilutions of secondary antibodies followed recommendations of the manufacturers.

To test staining for specificity against the respective antigenic epitope, hSGLT1-Ab or hSGLT2-Ab was incubated for 4 h at room temperature with the respective immunizing peptide (0.3–0.5 mg/ml) before using them for immunostaining.

After staining, sections were overlayed with Vectashield, coverslipped, sealed with nail polish, and inspected for immunofluorescence. Sections shown in most immunocytochemical figures were examined with an Opton III RS fluorescence microscope (Opton Feintechnik, Oberkochen, Germany) and photographed using a software-guided digital camera Spot RT Slider (Diagnostic Instruments, Sterling Heights, MI, USA). Sections shown in Fig. 7 were examined by laser scanning fluorescence microscopy as described [16]. The confocal laser scanning image system LSM510 from Zeiss (Jena, Germany) was employed using the argon laser for green fluorescence (λ_{ex}=488 nm, LP 505 nm) and the helium–neon laser for red fluorescence (λ_{ex}=543 nm, Bp 560–612 nm). For examination, the Zeiss LSM-510 software 2.5 SP2 stack, multi-track, 8 bit scan mode was used.

The images were imported into Adobe Photoshop 6.0 for processing and labeling. In some images, fluorescence obtained after staining with one fluorescent antibody was converted into black and white mode using the same software.

Preparation of total cell membranes from cells and tissues

Cell suspensions and tissues were homogenized using a Powergen 125 homogenizer (Fischer Scientific), and TCM were isolated by differential centrifugation as described [2, 42, 44]. TCM from the kidney were isolated from the cortex and outer stripe tissues. Human jejunum was open longitudinally, rinsed with cold PBS, and the mucosa was collected by

scraping. For preparation of TCM from homogenates, cell debris was removed by 15-min centrifugation at 6,000×*g*, and TCM (pellet) were collected by centrifugation of the supernatant for 1 h at 150,000×*g*. The TCM preparations were resuspended in 150 mM mannitol, 2.5 mM EGTA, 12 mM Tris/HCl, pH 7.4, and stored at −70 °C until use. Protein was measured by the dye-binding assay [7].

SDS-PAGE and Western blotting

Sample treatment for SDS-PAGE and conditions for immunoreactions with hSGLT1-Ab and hSGLT2-Ab in Western blots were processed in details described previously [2, 42, 44]. The same conditions were used for both antibodies. In short, proteins were mixed with Laemmli buffer in the absence of reducing agent, denaturated for 15 min at 65 °C, separated by SDS-PAGE in 10 % acrylamide mini gels, and wet-transfered to Immobilon membrane (Millipore, Bedford, MA). The Immobilon membranes were incubated with hSGLT1-Ab (1:1,000 in blotting buffer), hSGLT2-Ab (1:1,000), or actin-Ab (0.5 μg/ml) overnight in a refrigerator, rinsed in antibody-free blotting buffer, incubated in blotting buffer containing 0.1 μg/ml GAR-AP or 0.5 μg/ml GAM-AP, respectively, rinsed, and stained for alkaline phosphatase activity using the 5-bromo-4-chloro-3-indolyl phosphate (BCIP)/nitro blue tetrazolium (NBT) assay. The labeled protein bands were evaluated by densitometry as described [2, 44]. To demonstrate the specificity for antigenic epitope, hSGLT1-Ab, hSGLT1-comAb, and hSGLT2-Ab were preincubated for 4 h at room temperature with 0.5 mg/ml of the respective peptide used for immunization before performing immunoreaction.

RT-PCR

RNA concentration was determined and cDNA was synthesized using iScript cDNA synthesis kit (Bio-Rad, CA, USA) according to the manufacturer's instructions. RT-PCR was performed according to iQ SYBR-Green Supermix RT-PCR system protocol (Bio-Rad, CA, USA). Initial denaturation was performed at 95 °C for 3 min. PCR amplification cycle was performed as follows: denaturation step at 95 °C for 15 s, annealing step at 59 °C for 30 s, and elongation step at 72 °C for 30 s. The latter cycle was repeated 45 times. The nontemplate control reactions, where the cDNA is substituted with DNase/RNase-free water, were included in each PCR reaction indicating the absence of possible contamination. Primers used for RT-PCR reactions were created to span introns in order to avoid false-positive results due to contamination with genomic DNA by using PrimerBLAST software (www.ncbi.nlm.nih.gov). The sequences of specific primers used for RT-PCR reactions and predicted RT-PCR product sizes are indicated in Table 1. The RT-PCR products were tested for correct size by melting point analysis and agarose gel electrophoresis. Subsequently, the respective PCR products were excised, extracted, and analyzed in a 3130 Genetic Analyzer (Applied Biosystems, CA, USA).

Presentation of data and statistical analysis

The presented immunocytochemical pictures are representative for three to four independent tissue samples, whereas the densitometric values shown in Fig. 5b, d represent means± SEM of Western blot data obtained with TCM samples isolated from eight male and six female kidneys. Statistical significance of differences between females and males was evaluated by Student's *t* test at 5 % significance level.

Results

Novel subtype-selective polyclonal antibodies against hSGLT1 and hSGLT2

The SGLT subtype selectivity of the novel antibodies against hSGLT1 and hSGLT2 was analyzed using BHK-21 cells that were stably transfected with hSGLT1, hSGLT2, or hSGLT3. BHK-21 cells stably transfected with the human H^+-peptide cotransporter hPEPT1 were used as negative control. Effective expression was verified by Northern blotting (hSGLT1, hSGLT2, hSGLT3, hPEPT1; data not shown), by immunocytochemistry and Western blotting (Fig. 1: hSGLT1, hSGLT2, hSGLT3) using the novel antibodies against hSGLT1 and hSGLT2 and a previously described antibody against hSGLT3 [12], and by uptake measurements using [^{14}C]α-methylglucopyranoside (hSGLT1, hSGLT2) or [^{3}H]glycylglycine (hPEPT1) (data not shown). To compare the hSGLT-subtype selectivity in immunocytochemistry, the stably transfected cells were processed using the same protocol as the investigated human tissues. Figure 1 shows subtype-specific immunocytochemical staining of hSGLT1 by hSGLT1-Ab, of hSGLT2 by hSGLT2-Ab, and of hSGLT3 by hSGLT3-Ab. The same result was observed for immunolabeling of 70–80 kDa protein bands in Western blots of TCM that had been isolated from the transfected cells. With both methods, no cross-reactivity was observed among the antibodies.

Identification of organs with distinct expressions of hSGLT1 and hSGLT2 using RT-PCR

To focus our immunocytochemical studies to human tissues which show distinct expression of hSGLT1 and/or hSGLT2 on the mRNA level, we analyzed the mRNA expression of hSGLT1 and hSGLT2 in kidney, small intestine, heart, liver,

Table 1 Primer sequences used for RT-PCR

Gene	Primers (5′–3′)	NCBI accession no.	Location	RT-PCR product (bp)
hSGLT1 (SLC5A1)	F: GCATCGCCTGGGTGCCCATT R: GCACCGTGCTGCTCTAGCCC	NM_000343.3 mRNA	1560-1579 2081-2100	541
		NT_011520.12 DNA	11885768-11885787 11896605-11896624	10,857
hSGLT2 (SLC5A2)	F: GGTGCTGCTACTGGGCTGGC R: TCCCACGGCTGGATCCTCGG	NM_003041.3 mRNA	334-353 747-766	433
		NT_010393.16 DNA	31437061-31437080 31438923-31438942	1,882
hβActin (ACTB)	F: ACAGAGCCTCGCCTTTGCCG R: GACGCAGGATGGCATGGGGG	NM_001101.3 mRNA	30-49 597-616	587
		NT_007819.17 DNA	5560155-5560174 5558350-5558369	1,435

lung, adipose tissue, and different brain regions (Fig. 2). As expected [55], *hSGLT1* mRNA was detected in kidney and small intestine, whereas a strong *hSGLT2* mRNA signal was observed only in kidney. Consistent with the literature [8, 59], we also obtained distinct hSGLT1-related RT-PCR signals in heart, liver, and lung. The identity of the amplification products with hSGLT1 was verified by DNA sequencing. Under the employed experimental conditions, no hSGLT1-related RT-PCR signals were obtained in adipose tissue and brain.

Localizations of hSGLT1 and hSGLT2 in human kidney

Using the novel antibodies against hSGLT1 and hSGLT2, we first investigated expression of these transporters in human kidney. Figure 3 shows that the nephron distribution of hSGLT1 and hSGLT2 is similar to that in rodents, showing expression of hSGLT2 protein in the proximal tubule S1 and S2 segments and expression of hSGLT1 in the proximal tubule straight (S3) segment [2, 44]. Both transporters were clearly localized to the brush border membrane (BBM) (Fig. 3b, c, d, e, g, i). Immunostaining of proximal tubules by hSGLT1-Ab and hSGLT2-Ab in sections (Fig. 3h, j) and of ~75 kDa bands in Western blots of TCM (Fig. 3k, l) could be blocked by the antigenic peptides. A double immunostaining with hSGLT1-Ab and hSGLT2-Ab indicated that the expression of hSGLT1 and hSGLT2 has no overlap between nephron segments (compare Fig. 3a, d and b, f). Various blood vessels remained unstained with either hSGLT antibody (data not shown).

In view of our recent findings in rats, where rSglt1 was localized also in the luminal membrane of macula densa and thick ascending limb of Henle (TALH) cells [2], we have

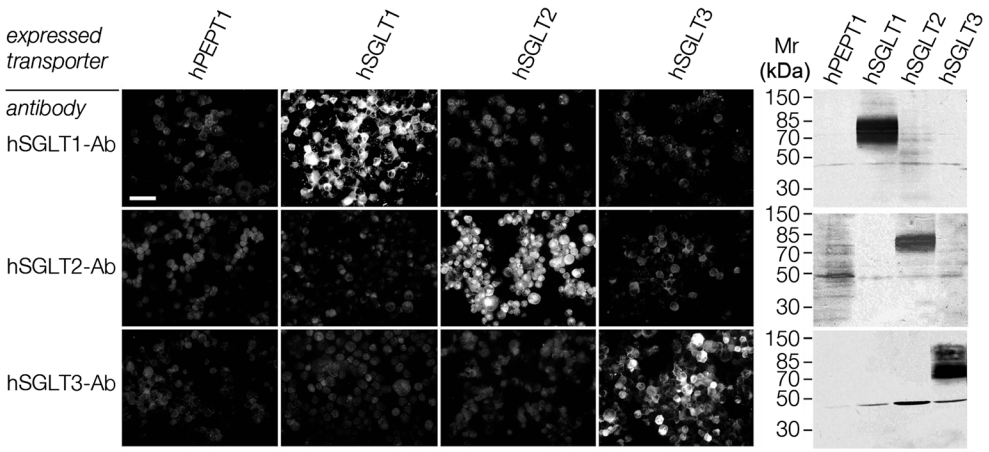

Fig. 1 Demonstration that hSGLT1-Ab and hSGLT2-Ab react subtype-specific in immunocytochemistry and Western blots. Subtype specificity of hSGLT1-Ab and hSGLT2-Ab, and of a previously described antibody against the homologous glucose sensor hSGLT3 [12], was tested by immunocytochemistry using PFA-fixed BHK-21 cells (*left panel*). The BHK-21 cells were stably transfected with the indicated transporters using cells that were transfected with the human H^+-peptide cotransporter hPEPT1 as negative control. For immunocytochemistry, cells were smeared on glass slides, fixed with PFA, and an antigen retrieval and antibody staining were performed as described for tissue cryosections. On the *right panel*, Western blots are shown that were performed with total cell membranes (TCM) isolated from the transfected BHK-21 cells. *Bar*, 20 μm

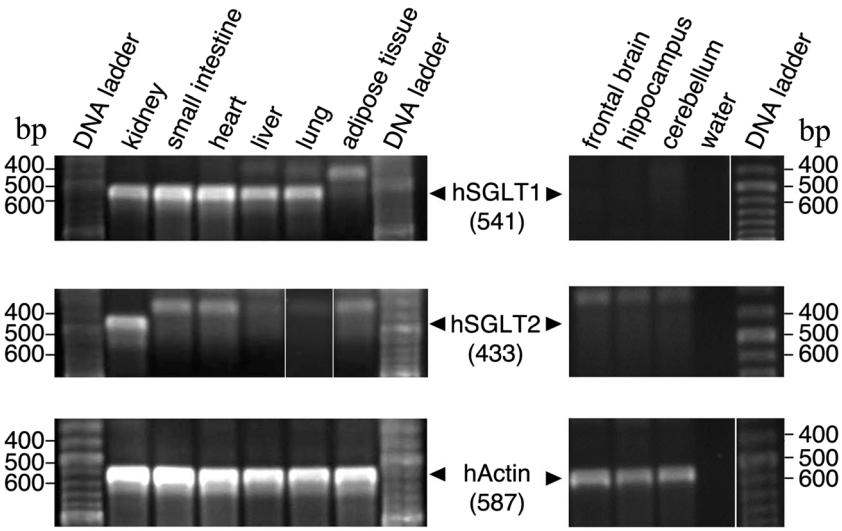

Fig. 2 Expression of *hSGLT1* and *hSGLT2* mRNAs in several human tissues. RT-PCR was performed on human RNAs purchased from Clontech (USA) using the primers shown in Table 1. Agarose gel electrophoresis of the RT-PCR products indicates the sizes of the expected amplification products. The identity of the amplified *hSGLT1* fragments (541 bp) in kidney, small intestine, heart, liver, and lung and of the amplified *hSGLT2* fragments in kidney (433 bp) was verified by nucleotide sequencing

performed a more detailed localization of both hSGLT1 and hSGLT2 proteins along the human nephron (Fig. 4). As shown in the panel hSGLT1 (Fig. 4a–f), the hSGLT1-Ab-related immunoreactivity was detected exclusively in the

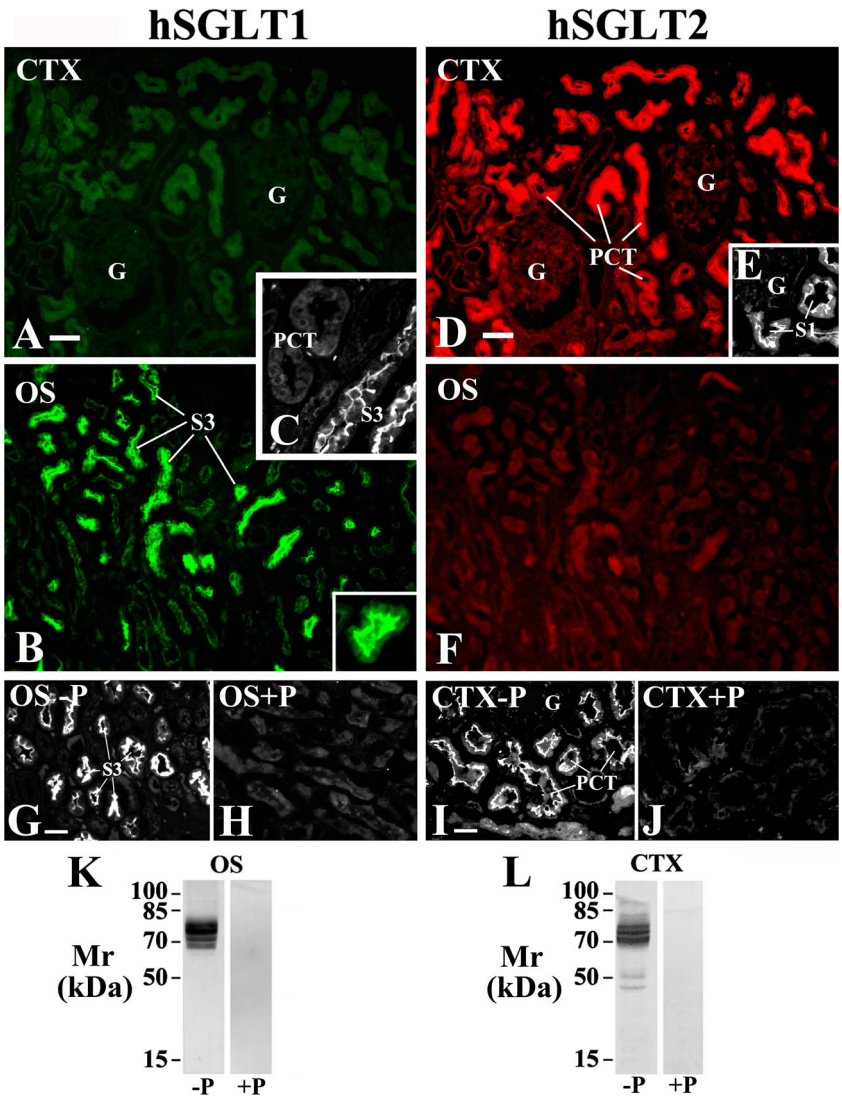

Fig. 3 Localization of hSGLT1 and hSGLT2 proteins in human kidney, as shown in double- and mono-stained cryosections; effect of immunizing peptide-blocked antibodies. In double-stained mode (**a**–**f**), sections were first stained with hSGLT1-Ab and GAR-FITC (**a**–**c**, *green fluorescence*), then with hSGLT2-Ab and GAR-CY3 (**d**–**f**, *red fluorescence*). In mono-stained mode (**g**–**j**), sections were stained with native (**g**) or peptide-blocked (**h**) hSGLT1-Ab or with native (**i**) or peptide-blocked (**j**) hSGLT2-Ab. *CTX*, cortex; *OS*, outer stripe; *G* glomeruli; *PCT*, proximal convoluted tubule (S1/S2 segments); *S3*, proximal tubule straight segments in medullary rays (**c**) and OS; *P*, immunizing peptide. *Bars*, 20 μm. The Western blots in K and L were preformed with TCM that had been isolated from OS or CTX. The immunolabeling in Western blots was performed with hSGLT1-Ab (**k**) or hSGLT2-Ab (**l**) with native (−*P*) or peptide-blocked (+*P*) antibodies. Per lane, 60 μg of protein was applied

proximal tubule S3 segments in medullary rays (d) and outer stripe (e). The cells in other nephron segments, including macula densa (b) and TALH (c–f), remained unstained. As shown in the panel hSGLT2 (Fig. 4a*–f*), the hSGLT2-Ab-related immunoreactivity was detected only in the cortical proximal tubules, e.g., in the S1 segment (Fig. 4a*) and S1/S2 segments of the proximal convoluted tubules (PCT; Fig. 4a*–c*), whereas the staining in other nephron segments, including macula densa, was absent.

Similar staining patterns were observed in sections obtained from male and female kidneys. To determine whether the expression levels for hSGLT1 and hSGLT2 in human kidneys are sex-dependent, as observed for these transporters in rodents [2, 42, 44], we compared the hSGLT1 protein abundance in TCM from renal outer stripe and hSGLT2 protein abundance in TCM from renal cortex in Western blots (Fig. 5). Different to rats and mice, no sex difference in the expression of hSGLT1 and hSGLT2 proteins was detected.

Localization of hSGLT1 in enterocytes of human small intestine

In Western blots of TCM isolated from human intestinal mucosa, the hSGLT1-Ab labeled a single broad protein band of 70–80 kDa, which was absent after blocking the antibody with the antigenic peptide (Fig. 6a). Immunostaining of SGLT1 in human small intestine was similar as described in rats [2, 18, 48]; with hSGLT1-Ab, the brush border of jejunal enterocytes in villi was heavily stained (Fig. 6b, d, e). Similar to Western blots, the immunocytochemical staining was blocked with the antigenic peptide (Fig. 6c and inset in 6d). We often observed a punctuate intracellular staining below the

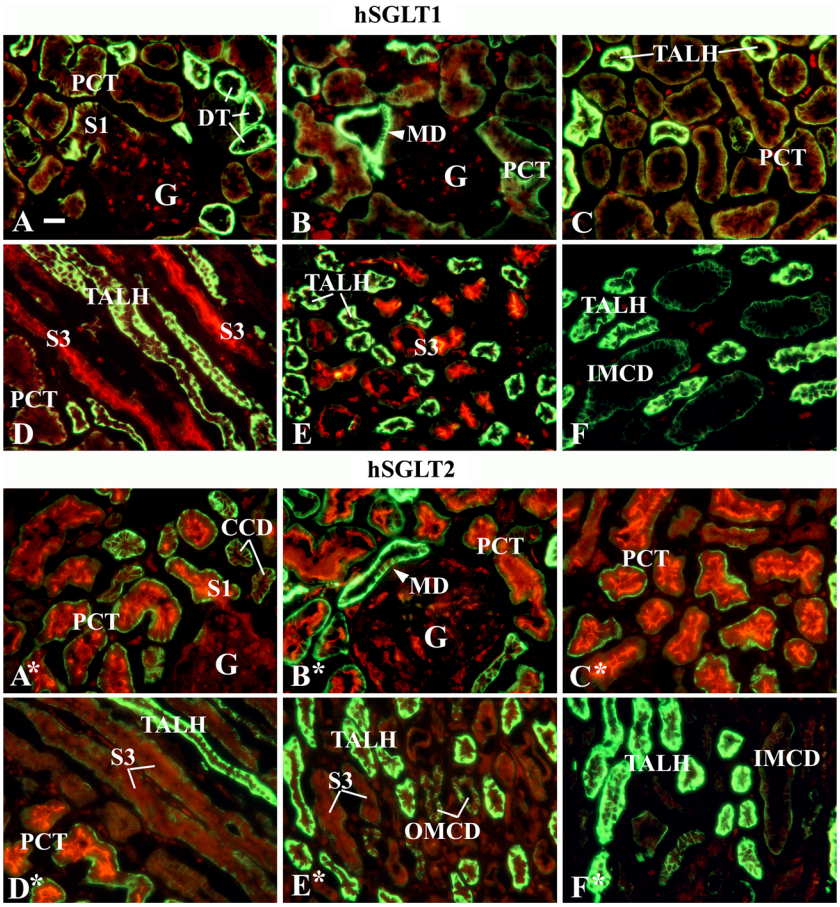

Fig. 4 Double staining of hSGLT1 (*red fluorescence*) and the Na/K-ATPase (*green fluorescence*) (*upper panel*, **a**–**f**) and hSGLT2 (*red fluorescence*) and the Na/K-ATPase (*green fluorescence*) (*lower panel*; *a**–*f**) in various segments of the male human nephron. **a** and *a**, **b** and *b**, superficial cortex; **c** and *c**, deep cortex; **d** and *d**, medullary rays; **e** and *e**, outer stripe; **f** and *f**, inner stripe. *G*, glomerulus; *PCT*, proximal convoluted tubules; *S1*, the initial proximal tubule segment; *S3*, proximal tubule straight segment; *TALH*, thick ascending limb of Henle; *MD*, macula densa; *DT*, distal tubule; *CCD*, cortical collecting duct; *OMCD*, outer medullary collecting duct; *IMCD*, inner medullary collecting duct. *Upper panel*: hSGLT1 was stained exclusively in the BBM of S3 segments in medullary rays (**d**) and outer stripe (**e**). Glomeruli (**a** and **b**), various PCT profiles in the cortex (**a**–**c**), macula densa (**b**), TALH in various zones (**c**–**f**), and cortical distal tubules (**a**) were variably stained for Na/K-ATPase but were negative for hSGLT1. *Lower panel*: hSGLT2 was strongly stained in the BBM of S1 and other cortical PCT profiles (*a**–*c**), but the S3 segments in medullary rays (*d**) and outer stripe (*e**) remained unstained. Other nephron segments in the cortex (*a**–*c**) and outer (*e**) and inner stripe (*f**) were also negative for hSGLT2. *Bar*, 20 μm for all images

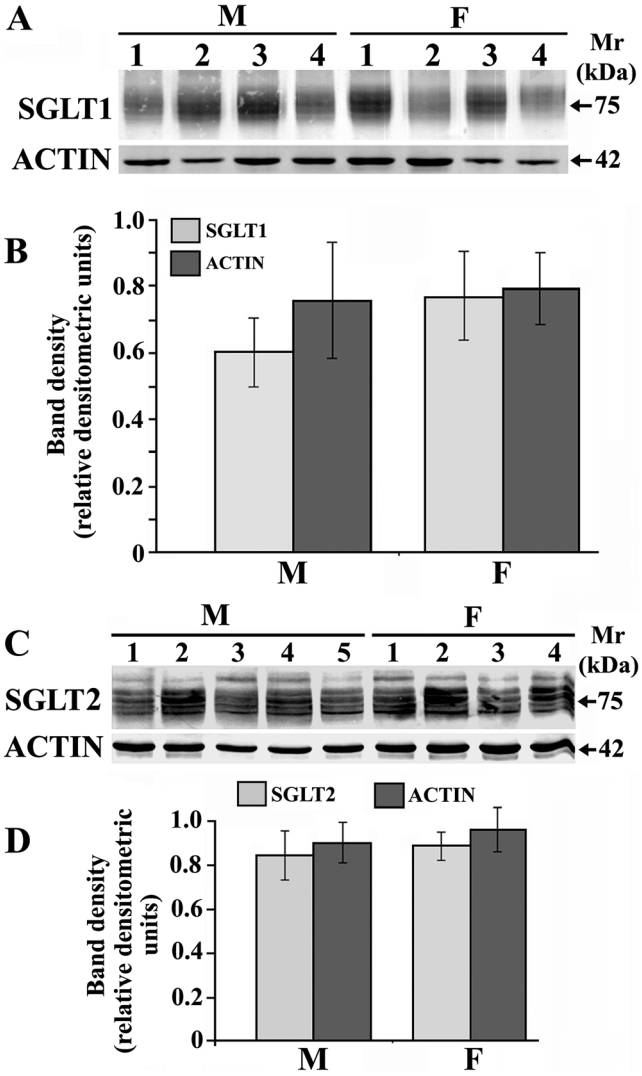

Fig. 5 Abundance of hSGLT1 and hSGLT2 protein in TCM isolated from outer stripe (**a**, **b**) and cortex (**c**, **d**) of the human male and female kidneys. Western blots were labeled with hSGLT1-Ab (**a**) or hSGLT2-Ab (**c**) and were performed with 40 μg protein per lane. Labeling with actin-Ab was used as a loading control. The representative Western blots are shown in **a** and **c**, whereas the densitometric quantifications of the hSGLT-related ~75 kDa protein bands, and of the actin-related ~42 kDa band, are shown in **b** and **d**. The data in **b** and **d** were collected from two independent experiments with different membrane preparations from a total of eight male and six female kidneys. No significant differences between males and females were observed

enterocyte brush border (Fig. 6e, arrows). This staining suggests that hSGLT1 is associated with subapical vesicles, which may contribute to posttranscriptional regulation of SGLT1 via endocytotic and exocytotic events [54, 56]. Figure 6f shows that hSGLT1-Ab also stained the brush border of the cells in crypts. Blood vessels in various intestinal segments remained unstained with hSGLT1-Ab (data not shown). Like in rats, the staining distribution and intensity of hSGLT1 in human small intestine were similar in men and women (data not shown).

Localization of hSGLT1 in K and L Cells of human small intestine

In mice, the expression of mSglt1 has been described in K and L cells of small intestine, and data have been reported which suggest that mSglt1 mediates a glucose-dependent secretion of insulinotropic hormone (GIP) in K cells and glucagon-like peptide 1 (GLP-1) in L cells [16, 34, 38]. Here, we investigated whether hSGLT1 is expressed in K and L cells of human intestine. We performed double staining with rabbit-raised hSGLT1-Ab and either a goat-raised GIP-Ab or GLP-1-Ab. The immunoreactions were visualized with fluorophore-labeled secondary antibodies against rabbit or goat. The fluorescence was visualized by laser scanning microscopy using an optical section thickness of 0.1 μm. In Fig. 7, enteroendocrine cells are shown in which coexpression of hSGLT1 with GIP or GLP-1 was detected. K cells expressing hSGLT1 and GIP were observed in villi (Fig. 7a) and crypts (Fig. 7b). In these cells, hSGLT1-related immunoreactivity was always detected at the apical cell domain. In some cells, a limited immunoreactivity of hSGLT1-Ab was also associated with GIP-Ab-positive intracellular compartments (Fig. 7b). L cells expressing hSGLT1 and GLP-1 were also observed in villi (Fig. 7c, d) and crypts (not shown). Also in the L cells, hSGLT1 was always located at the apical cell domain (Fig. 7c, d). For GLP-1 containing intracellular compartments, different hSGLT1-Ab immunoreactivity was observed, varying from no (not shown) to weak (Fig. 7c) or strong (Fig. 7d) staining.

Localization of hSGLT1 in biliary duct cells of human liver

In liver, hSGLT1-Ab stained bile duct epithelial cells (Fig. 8a, arrows). The immunostaining was observed at the apical membrane and in intracellular organelles (Fig. 8a, inset). Staining of the bile ducts with hSGLT1-Ab was blocked with the antigenic peptide (Fig. 8b). Hepatocytes (Fig. 8a, b, arrowheads) and small or large blood vessels (Fig. 8a, asterisk) exhibited no staining.

Localizations of hSGLT1 in alveolar type 2 cells and in Clara cells of human lung

In peripheral tissue of human lung, individual polymorphic cells in alveolar walls were strongly stained with hSGLT1-Ab (Fig. 9a, arrows). This staining was blocked by antigenic peptide (Fig. 9b). To distinguish whether the stained cells represent macrophages (dust cells) or alveolar type 2 cells, we performed double staining with hSGLT1-Ab and with an antibody to CD68 protein (CD68-Ab) in macrophages [49] (Fig. 9c–e). The hSGLT1-positive cells (Fig. 9c, arrowheads), which seem to represent the surfactant-producing type 2 alveolar cells, were different from the CD68-positive

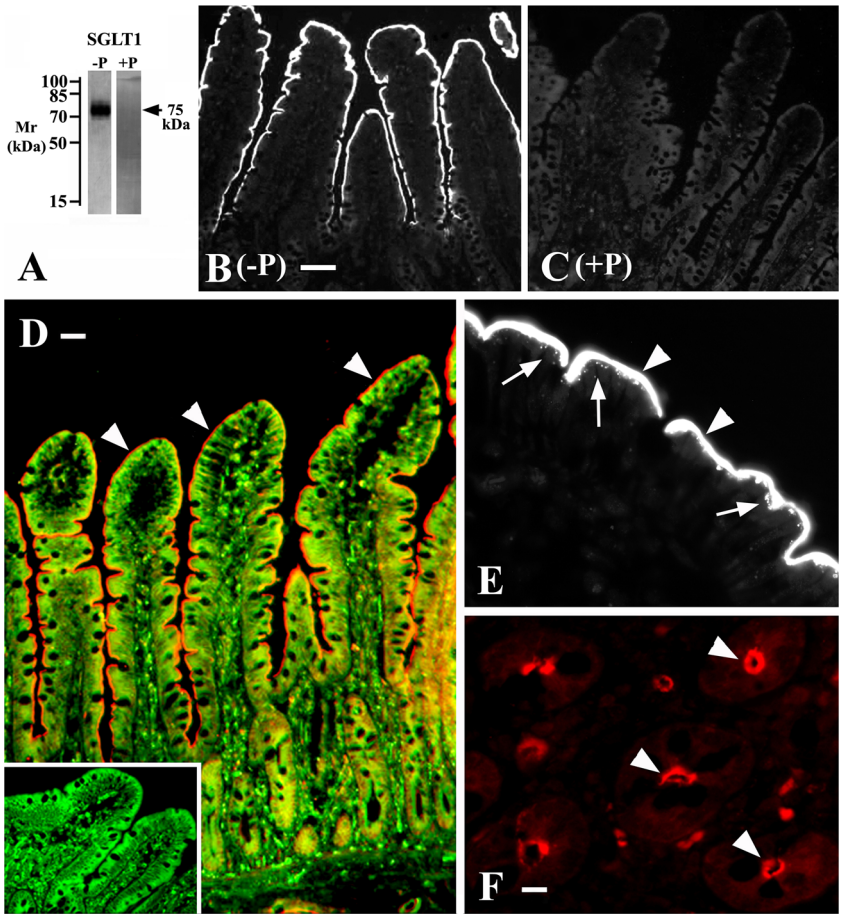

Fig. 6 Immunocytochemical localization of hSGLT1 in enterocytes of human small intestine. **a** Western blot of TCM isolated from jejunum of male humans. The blot was stained with native (−*P*) or immunizing peptide-blocked (+*P*) hSGLT1-Ab. Each lane contained 40 μg protein. The native antibody labeled the ~75-kDa protein band, which was absent after the antibody had been blocked by the peptide. **b**, **e**, **f** Immunostaining of tissue cryosections with native hSGLT1-Ab (−*P*). **c** Immunostaining with the peptide-blocked (+*P*) hSGLT1-Ab. **d** Double staining with hSGLT1-Ab (*red*) and actin-Ab (*green*). Strong immunoreactivity of the enterocyte brush border membrane (*BBM*) in villi (**b**, **d**, and **e**, *arrowheads*) and crypts (**f**, *arrowheads*) could be blocked by the antigenic peptide (**c** and *inset* in **d**). Large magnification indicated punctuated hSGLT1-Ab staining of enterocytes below the BBM (**e**, *arrows*). *Bars* 50 μm (**b** and **d**) or 25 μm (**f**)

macrophages (Fig. 9d, arrowheads), as clearly shown in the merged c and d figures (Fig. 9e). In the hSGLT1-positive cells, immunoreactivity was localized predominantly in the densely populated intracellular organelles (inset in Fig. 9c).

Immunostaining of bronchioles with hSGLT1-Ab revealed nonspecific staining of peribronchial elastical fibers (Fig. 10a, arrows, and c–h) that was not blocked by the antigenic peptide (Fig. 10b). In contrast, peptide-blockable immunostaining with SGLT1-Ab was observed at the luminal membrane of some bronchiolar epithelial cells (arrowheads in Fig. 10a, c, e, f, h). Double staining with hSGLT1-Ab and tubulin-Ab (Fig. 10c–e) indicated that the hSGLT1-Ab-positive cells (C-E, arrowheads) are different from the tubulin-positive ciliated cells (c–e, arrows), suggesting that they represent Clara cells. Employing double staining with hSGLT1-Ab and an antibody against the protein CC10, which is secreted by Clara cells [20, 46], SGLT1-Ab immunoreactivity of the Clara cells was verified. In some Clara cells, strong immunoreactivity of hSGLT2-Ab was localized apically, and CC10-Ab immunoreactivity was observed in the subapical domain of the same cells (Fig. 10f–h). In another population of Clara cells, which were randomly distributed among the ciliated cells (Fig. 10i–k), a strong peptide-blockable immunoreactivity with CC10-Ab and hSGLT1-Ab colocalized in intracellular organelles (Fig. 10l–n, arrowheads). Performing immunocytochemical studies with a commercial polyclonal antibody against hSGLT1 raised in goat (hSGLT1-comAb), we confirmed the localization of hSGLT1 in Clara cells and alveolar type 2 cells (Online Resource Fig. S1). To evaluate for potential species differences, we also investigated the expression and location of rSglt1 in rat lung (Online Resource Fig. S2). For immunolocalization of rSglt1 in rat lung, we used the previously characterized antibody rSglt1-Ab [2]. Similar to human, we localized rSglt1 in Clara cells and alveolar type 2 cells.

Localization of hSGLT1 in capillaries of human heart

Immunostaining of sections of human myocard with hSGLT1-Ab revealed distinct staining of elongated structures between myocytes that could be blocked by antigenic peptide (Fig. 11a, b, arrows). Double staining with AQP1-Ab and Na/K-ATPase-Ab showed that the elongated structures between myocytes were also positive for AQP1 which binds to endothelial cells of heart capillaries [40, 41] (Fig. 11c–e, large arrows), whereas Na/K-ATPase-positive sarcolemma and intercalated discs (Fig. 11d, arrowheads and thin arrows) were

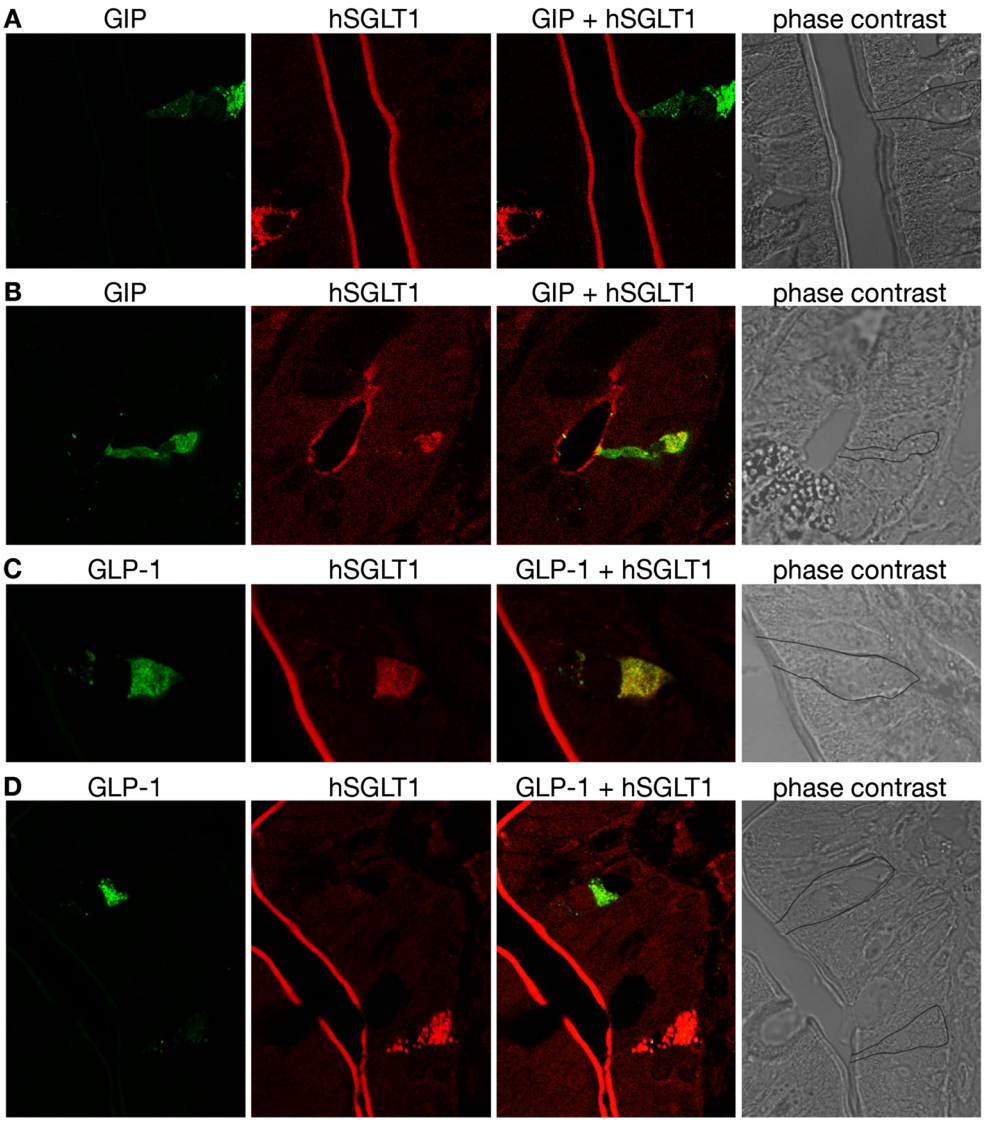

Fig. 7 Expression of hSGLT1 in enteroendocrine K cells secreting GIP and L cells secreting GLP-1. Sections from small intestine of male humans were first incubated with the antibodies against GIP (GIP-Ab) or GLP-1 (GLP-1-Ab) that were raised in goat, followed by the respective FITC-labeled secondary antibody (*green*), and then with hSGLT1-Ab raised in rabbit, followed by the CY3-labeled secondary antibody (*red*). Fluorescence was observed by laser scanning fluorescence microscopy using an optical section thickness of 0.1 μm. Phase contrast microscopy was performed to facilitate identification of the cell borders of stained enteroendocrine cells. **a** K cell in a villus coexpressing hSGLT1 at the luminal membrane. The pictures also show one cell in the villus expressing hSGLT1 at intracellular compartments. **b** K cell in a crypt coexpressing hSGLT1 at the BBM and at intracellular compartments. **c** L cell in a villus coexpressing hSGLT1 at the BBM and at intracellular compartments. **d** L cell in a villus coexpressing hSGLT1 at the BBM. The picture also shows a cell at the transition between villus and crypt expressing hSGLT1 at the BBM and at intracellular compartments

negative for AQP1 (Fig. 11e). Double staining with hSGLT1-Ab and Na/K-ATPase-Ab (Fig. 11f–h) showed that hSGLT1-Ab does not bind to plasma membranes and intercalated disks of myocytes suggesting that the hSGLT1-Ab-positive

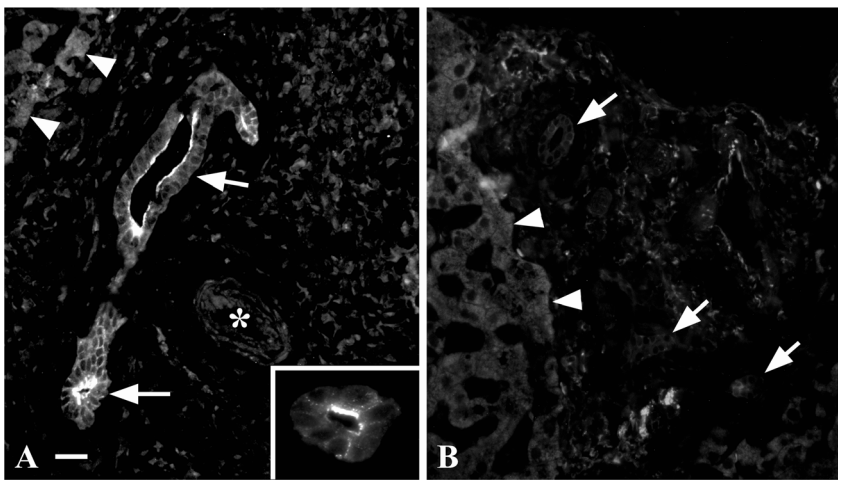

Fig. 8 Localization of hSGLT1 in human liver. The liver cryosections were immunostained with the native (**a**) or peptide-blocked hSGLT1-Ab (**b**). Bile duct cells are indicated by *arrows*, hepatocytes by *arrowheads*, and a small blood vessel by an *asterisk*. Peptide-blockable hSGLT1-Ab immunoreactivity was observed at the apical domain of bile duct cells. In these cells, a vesicular-type staining with hSGLT1-Ab was also observed in some intracellular organelles (inset in **a**). *Bar*, 20 μm

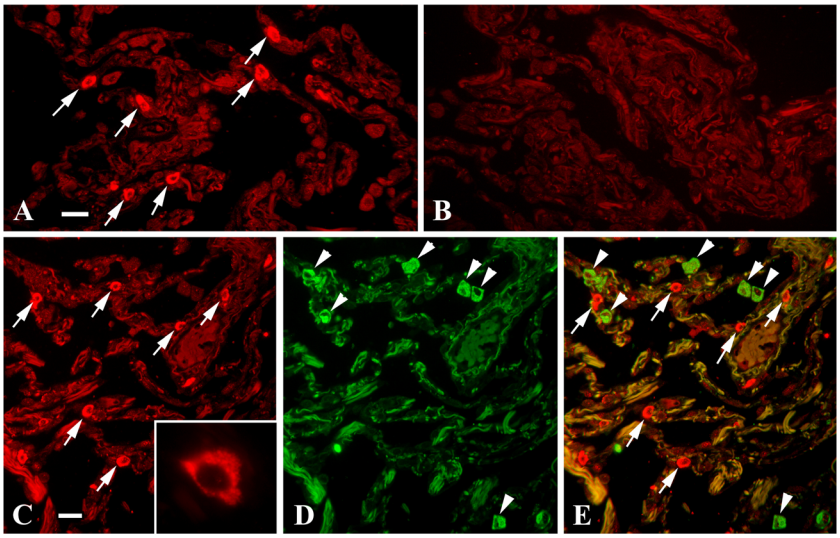

Fig. 9 Localization of hSGLT1 in alveoles of human lung. **a** Peripheral lung tissue was immunostained with hSGLT1-Ab. **b** Immunostaining was performed with the antigenic peptide-blocked hSGLT1-Ab. **c**–**e** Double immunostaining for hSGLT1 and macrophage marker protein CD68. Cryosections of the peripheral lung tissue were first immunostained with SGLT1-Ab and GAR-CY3 (**c**) and then with CD68-Ab and GAM-FITC (**d**). The images in **c** and **d** are merged in **e**. Red alveolar cells stained by hSGLT1-Ab are indicated by *arrows*. They are differentiated from macrophages which are *green-stained* by CD68-Ab (*arrowheads*). The cells stained by hSGLT1-Ab represent alveolar type 2 cells in which hSGLT1 is associated with densely packed intracellular organelles (*inset* in **c**). *Bars*, 20 μm

elongated structures represent microvessels. Because both hSGLT1-Ab and AQP-1-Ab were raised in rabbits, and the immunoreactivity with the hSGLT1-Ab in the heart tissue was for unknown reason sensitive to heating and relatively weak, double staining with these antibodies was difficult to perform. We thus performed double staining with a commercial polyclonal peptide antibody against hSGLT1 raised in goat (hSGLT1-comAb) and AQP1-Ab (Fig. 11i–k). Colocalization of immunoreactivity with hSGLT1comAb and AQP1-Ab (Fig. 11k) confirmed that hSGLT1 is colocalized in the AQP1-positive [40, 41] endothelial cells of the heart capillaries.

In a previous publication, we described peptide-blockable immunoreactivity of an antibody raised against a peptide of rat Sglt1 in small vessels of heart muscle [14]. Because we observed later that the antibody used in this study showed peptide-blockable cross-immunoreactivity with another protein in kidney [2], the localization of rSglt1 in small vessels of heart turned out to be ambiguous. Performing double immunostaining of cryosections from rat heart with a commercial antibody against rSglt1 raised in goat (rSglt1-comAb; Everest Biotech, Oxfordshire, UK; EB11236) and with the rabbit-raised AQP1-Ab, we also demonstrated immunoreactivity of rSglt1-comAb in endothelial cells of capillaries (Online Resource Fig. S3). The data thus indicate that in the human and rat heart, SGLT1 protein is localized in capillaries.

Discussion

In this manuscript, immunochemical characterization of SGLT1 and SGLT2 in human organs was determined employing new subtype-specific antibodies that can be used for Western blotting and immunostaining. With previously reported antibodies against SGLT1 and SGLT2, no high quality immunocytochemistry has been described in human tissues [11, 56]. Thus, the knowledge concerning the locations of hSGLT1 and hSGLT2 proteins in human was based on few in situ hybridization experiments [59] and on the assumption that the immunochemical data in other species represent the situation in humans [56]. Because selective inhibitors of SGLT2 that inhibit renal glucose reabsorption have been introduced for treatment of type 2 diabetes [1, 27–29, 32], and an inhibitor of SGLT1 that blocks small intestinal glucose absorption and increases secretion of GLP-1 has been proposed as new antidiabetic drug [37, 58], a detailed immunocytochemical localization of hSGLT1 and/or hSGLT2 in human kidney, small intestine, and other organs was overdue.

Employing the new antibodies, we localized hSGLT2 to BBM of the proximal tubule S1 and S2 segments and hSGLT1 to BBM of the straight (S3) segment. A similar nephron distribution has been observed in rats and mice [2, 19, 22, 26, 44]. However, at variance to rats [2] and mice (Vrhovac et al., unpublished data), in humans no immunoreactivities for hSGLT1 were observed in the luminal membrane of TALH and macula densa cells. So far, the functional role of Sglt1 in the macula densa of rodents has not been investigated. It is possible that Sglt1-mediated Na^+-D-glucose cotransport at high glucose concentrations in the distal tubule depolarizes macula densa cells and increases tubuloglomerular feedback (TGF) and/or renin secretion. It has been shown in diabetic rats that blockage of Sglt2 in the proximal tubule activated TGF and reduced glomerular filtration, and the authors

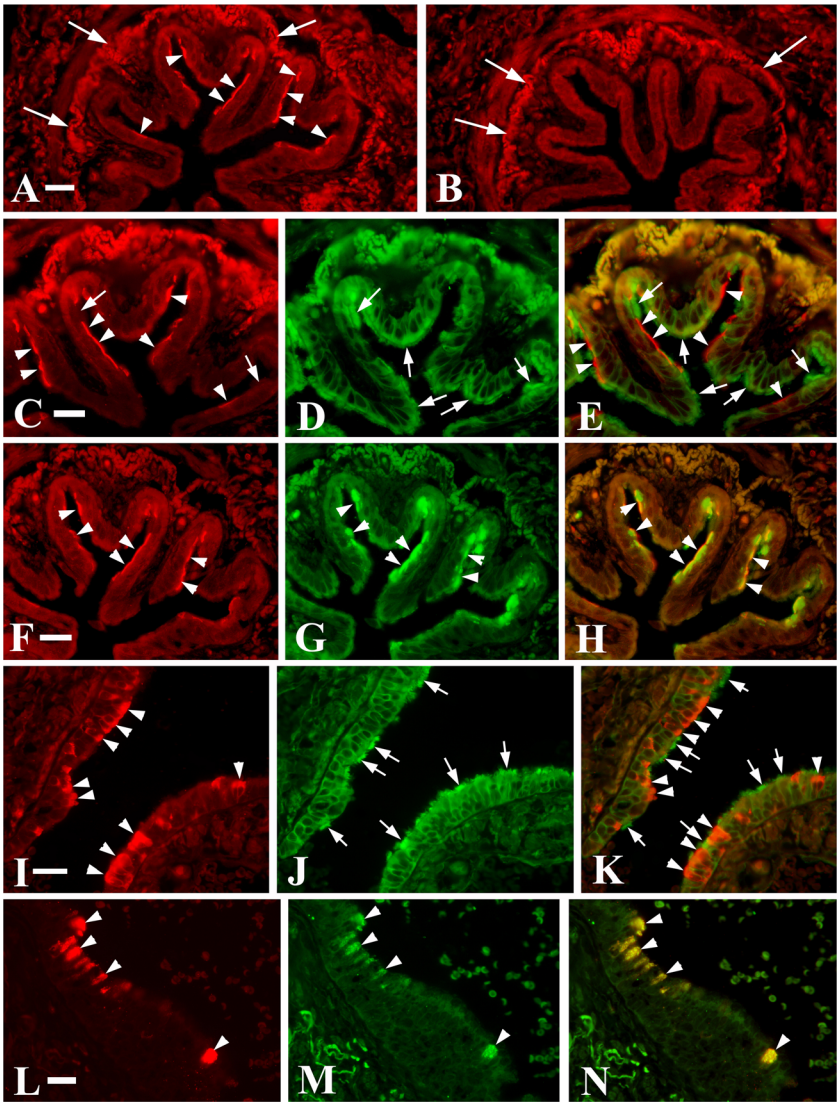

Fig. 10 Localization of hSGLT1 in terminal bronchioli of human lung. **a** Immunostaining of a bronchiolus with hSGLT1-Ab. Staining of the apical domains of epithelial cells is indicated by *arrowheads*. **b** Immunostaining of a bronchiolus with the immunizing peptide-blocked hSGLT1-Ab. The apical hSGLT1-Ab immunoreactivity in the epithelial cells was absent. The elastic fibers around bronchioli exhibited strong autofluorescence under red (**a**, *arrows*) or green fluorescence (**c**–**e**), which remained unchanged by the immunizing peptide (**b**, *arrows*), and were therefore considered nonspecific. **c**–**e** Double staining with hSGLT1-Ab (**c**) and tubulin-Ab (**d**) and merged **c** and **d** pictures (**e**). The cells expressing hSGLT1 (*arrowheads* in **c** and **e**) are different from the tubulin-positive ciliated cells (*arrows* in **d** and **e**). **f**–**h** Double staining with SGLT1-Ab (**f**, *arrowheads*) and CC10-Ab, a marker protein for Clara cells (**g**, *arrowheads*), and merged **f** and **g** images (**h**) indicate that hSGLT1 is expressed in Clara cells (*arrowheads*). In these Clara cells, staining of hSGLT1 is more apical compared to CC10, which is concentrated largely subapically (*arrowheads* in **h**). **i**–**k** Double staining with CC10-Ab (**i**, *arrowheads*) and tubulin-Ab (**j**, *arrows*) and merged images **i** and **j** (**k**). CC10-Ab-stained Clara cells (*arrowheads* in **k**) were randomly scattered among tubulin-positive ciliated cells (*arrows* in **k**). **l**–**n** In a group of Clara cells, the CC10-Ab-related (**l**, *arrowheads*) and hSGLT1-Ab-related (**m**, *arrowheads*) immunoreactivities were colocalized in intracellular organelles randomly scattered all over the cells, as indicated by *yellow staining* in merged **l** and **m** pictures (**n**, *arrowheads*). *Bars*, 20 μm for all images

speculated that this effect may be palliative for diabetic nephropathy [50, 52]. Because the activation of TGF after blockage of Sglt2 may not only be due to increased NaCl delivery to the macula densa but may be enhanced by increased delivery of glucose leading to Sglt1 mediated depolarization of macula densa cells, palliative effects of Sglt2 inhibitors on nephropathy may be only relevant for rodents. Because a small decrease of systolic blood pressure was observed after treatment of diabetic humans and mice with SGLT2 inhibitors [27, 32, 52], the Sglt1-mediated depolarization of macula densa cells may not be relevant for blood pressure. An additional difference in the expression of Sglts in rodents and SGLTs in humans is related to sex; in rats, higher expressions of rSglt1 and rSglt2 proteins were observed in the female kidney [2, 42, 44], and the male-dominant expression of mSglt2 protein was found in the mouse kidney [44], whereas in the human kidney, sex differences were not detected for both SGLTs (this study).

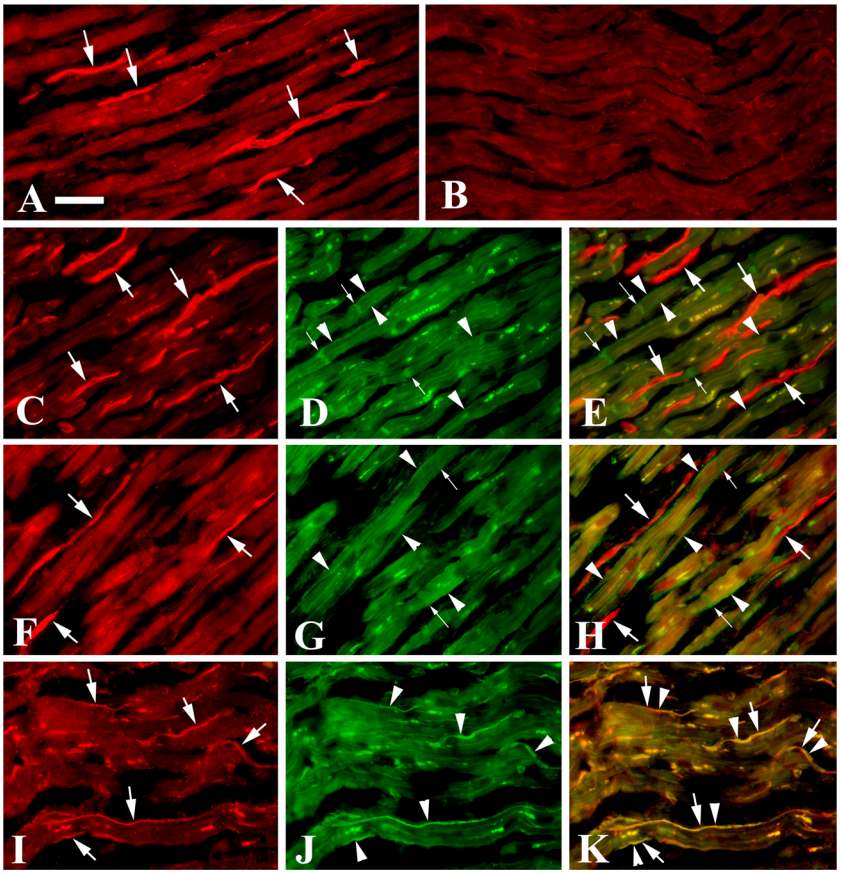

Fig. 11 Localization of hSGLT1 in human heart. **a** Immunostaining of human heart with hSGLT1-Ab revealed staining of elongated structures between muscle fibers. **b** This immunoreaction was blocked when hSGLT1-Ab had been preincubated with the antigenic peptide. **c**–**e** Double staining with an antibody against water channel AQP1-Ab, which is expressed in heart capillaries (**c**, *arrows*), and with Na/K-ATPase-Ab, which is expressed in the plasma membrane (sarcolemma) of heart muscle cells (**d**, *arrowheads*) and in intercalated discs (**d**, *thin arrows*). **e** Merged pictures **c** and **d**. The data showed that these two antibodies could be used to distinguish between the AQP1-positive capillaries and Na/K-ATPase-positive plasma membranes in human heart. **f**–**h** Double staining with hSGLT1-Ab (**f**, *arrows*) and Na/K-ATPase-Ab. **h** Merged picture of **f** and **g** showing that hSGLT1-Ab does not stain plasma membranes of myocytes and intercalated disks. **i**–**k** Double staining with the commercial antibody against hSGLT1 (EB09310-Ab) (**i**, *arrows*) and AQP1-Ab (**j**, *arrowheads*). **k** Merged picture of **i** and **j**, confirming that hSGLT1 and AQP1 are colocalized in heart capillaries (*yellow-stained structures*). *Bar*, 20 μm for all images

The use of new hSGLT1-Ab indicated in human small intestine a distribution similar to that in rodents [2, 18, 48]. In human jejunum, strong immunoreactivity for hSGLT1 was observed at the BBM of enterocytes in the villi, whereas less pronounced but significant immunoreactivity was obtained also at the BBM of enterocytes in the crypts. In human jejunum, we also observed hSGLT1-Ab immunoreactivity in a compartment below the BBM as has been also recognized in rats [18]. This subapical location is consistent with the intracellular location of hSGLT1 described in CaCo-2 cells which are frequently used as model for human enterocytes [24]. The location at intracellular vesicles of the enterocytes is also consistent with the observation that the amount of SGLT1 in the BBM increased rapidly after gavage of mice with glucose [16]. Employing laser scanning fluorescence microscopy in human small intestine, we determined a similar localization of hSGLT1 in GIP-expressing K cells and GLP-1-expressing L cells as in mice [16, 34, 38]. Whereas hSGLT1-Ab immunoreactivity was always observed in the luminal membranes of the cells expressing GIP or GLP-1, a colocalization of hSGLT1 with GIP or GLP-1 in intracellular vesicles was only observed in some cells. This heterogeneity may indicate different subpopulations or different functional states of K and L cells. It is a challenge for future studies to determine whether SGLT1 exhibits a functional role in intracellular vesicles loaded with GIP or GLP-1. The localization of hSGLT1 in the luminal membranes of K and L cells has biomedical relevance because inhibitors of SGLT1 are supposed to impair or block the glucose-dependent stimulation of the secretion of these enterohormones [33, 45]. The observation that in mice SGLT1 inhibitors decreased the GLP-1 concentration in the blood only within a narrow time window after glucose challenge but increased blood GLP-1 later on [16, 37] may be explained by inhibition of glucose absorption in the proximal small intestine leading to an increase of the glucose concentration in distal small intestine, where the GLP-1-secreting L

cells are localized. Bacteria in distal small intestine metabolize glucose to short chain fatty acids which are strong secretagogues of the L cells [37].

Potential sites of SGLT2 expression in addition to kidney, and of expression of SGLT1 in addition to small intestine and kidney, are of physiological interest and biomedical importance. The secondary active Na^+-D-glucose cotransporters may supply metabolic energy at sites with permanent or occasional high energy demand and may influence Na^+ gradients and water movements across membranes. Since the reversible inhibitors for SGLT2 employed for treatment of diabetes and the inhibitor of SGLT1 which is currently tested for treatment of diabetes enter the blood, they could inhibit SGLTs at locations other than kidney and intestine [1, 28, 29, 37, 58]. Considering the difficulty to perform unequivocal immunolocalization of proteins with low expression, we performed semiquantitative RT-PCR in some tissues where the expression of SGLT1 has been demonstrated in humans or animals in order to select tissues with high hSGLT1 expression for immunocytochemical investigation [5, 6, 8–10, 13, 17, 23, 25, 30, 36, 56, 57, 59]. We observed relatively large amounts of hSGLT1 mRNA in liver, heart, and lung but did not detect hSGLT1 mRNA in brain and fat tissue. Consistent with previous reports in humans and mice [8, 44, 55], we did not detect hSGLT2 mRNA in small intestine, liver, heart, lung, fat tissue, and brain. We do not claim that our negative results exclude any expression of SGLT1 and/or SGLT2 because very small mRNA amounts coding for these transporters may have not been detected in the investigated commercial RNA samples. In particular, we consider the possibility that small amounts of hSGLT1 are expressed in brain capillaries and/or in neurons as has been suggested for other species [2, 13, 36, 57].

As previously observed in rat [2], we detected hSGLT1 protein in biliary duct cells of human liver where it was located at the apical membrane. In rat, it has been shown that glucose enters the bile passively from hepatocytes and is reabsorbed in bile ducts by phlorizin-inhibitable Na^+-D-glucose cotransport [9, 17]. Employing an ex vivo study with bile duct units isolated from rat liver, it has been shown that the secondary active reabsorption of glucose in the bile ducts provides the osmotic driving force for water reabsorption via aquaporins [31]. This mechanism may explain the observation that the bile flow decreases in diabetic rats [8] and may contribute to cholestasis during diabetes. Applying a reversible SGLT1 inhibitor that enters the systemic circulation for the treatment of diabetes [37, 58] may increase the bile secretion and help to prevent cholestasis in the diabetic patients. However, increasing the glucose concentration in the bile fluid by blocking SGLT1 may increase the risk for bacterial infection.

In human lung, we localized hSGLT1 within epithelial cell type 2 in alveoles and within Clara cells in bronchioles. Twenty-five years ago, Basset and coworkers obtained the first evidence for SGLT-type transport in the lung. They described that phlorizin-inhibitable Na^+-D-glucose cotransport in perfused rat lung contributes to fluid absorption [4, 5]. In 1992, Kemp and Boyd reported that freshly isolated type 2 alveolar epithelial cells from guinea pig expressed phlorizin-inhibitable sodium-dependent transport of AMG, a specific substrate of SGLTs [23]. The present demonstration that SGLT1 is also expressed in type 2 alveolar cells in human suggests that the functional observations made in rodents are relevant for humans and that the observed phlorizin-inhibited AMG transport was mediated by SGLT1. The contribution of SGLT1 to fluid absorption in the peripheral lung suggests that inhibitors of SGLT1 reaching the blood may increase the amount of fluid in the alveoles and may increase the risk for bacterial infections. Because SGLT1-mediated glucose uptake may provide energy for the synthesis of surfactant, inhibitors of SGLT1 may also impair surfactant production.

In equine trachea, Joris and Quinton described glucose-induced short circuit currents that were blocked by phlorizin [21]. This suggested the expression of an SGLT-type transporter in the tracheal epithelium. At variance, Pezzulo and coworkers did not detect glucose-induced short circuit currents in cultivated human bronchial epithelial cells but presented data suggesting that glucose flux across bronchial epithelial cells is mediated via passive glucose transporters [35]. Because SGLT1 expression may have been lost during cultivation, or there may be a species difference between horse and human, it remained unclear whether SGLT1 is expressed in human tracheal and/or bronchial epithelial cells. In the present study, we showed that hSGLT1 is expressed in Clara cells where it is located at the luminal membrane and within an intracellular compartment. We also observed different expression levels and intracellular distributions of hSGLT1 in different subpopulations of Clara cells. The Clara cells are polymorphic and can transform into mucin-producing cells [15]. They build up most of the nonciliated cells in the bronchioles. Clara cells contain various cell subpopulations including stem cells which are important for the maintenance and repair of bronchiolar epithelium and may transform to cancer cells [39, 47]. In addition to mucin, the Clara cells secrete surfactant proteins, antimicrobiotic peptides, cytokines, and chemokines [39]. Via secretion of cytocrines and CC10 protein and other properties, they are involved in protection from environmental toxins and in control of inflammation [20, 47]. Future studies are required to determine whether hSGLT1 in the Clara cells contributes to glucose absorption in the bronchioles and in which subpopulations of the Clara cells hSGLT1 are expressed. It has to be investigated which of the different Clara cell functions depend on the SGLT1-mediated delivery of intracellular glucose.

Our finding that hSGLT1 is located in human heart capillaries has physiological and pathophysiological impact. The

presence of *hSGLT1* mRNA in human heart was first described by Zhou and coworkers [59] and later confirmed by others [3, 55]. In situ hybridization data in human heart, performed by Zhou and coworkers, were interpreted to indicate the presence of *hSGLT1* mRNA in cardiomyocytes. However, in the figure which they presented to demonstrate the *hSGLT1* mRNA expression in cardiomyocytes, strong hybridization signals can be seen in longitudinal structures that could represent blood vessels (see Fig. 5a in ref. [59]). Banerjee and coworkers also performed immunostaining of murine heart with the antibody against mSglt1; however, the presented pictures (see Fig. 1e in ref. [3]) do not allow to differentiate whether plasma membranes of myocytes or small vessels between myocytes were stained. The hSGLT1-staining of capillaries in human heart, observed with two different antibodies in the present work, is consistent with a previously performed immunocytochemical localization of rSglt1 in rat heart [14]. Because the antibody against rat Sglt1 used in that study turned out to show some nonspecific binding in rat kidney [2], we reevaluated the expression and localization of rSglt1 in rat heart using a commercial antibody against rSglt1. Since this antibody was raised in goat, it allowed double staining with an antibody against water channel AQP1 which is expressed in endothelial cells of heart capillaries. Although the amount of mRNA coding for SGLT1 is lower in rat compared to human, in rat, rSglt1 could be localized to heart capillaries. SGLT1 in the capillaries of heart muscle of human and rat may influence cardiac function. It has been shown that the contractive force of isolated muscle strips from human hearts without and with heart failure was increased by insulin in the presence of glucose, and this insulin-induced increase was reduced when the passive glucose transporter GLUT4 or SGLT1 was inhibited [54]. Given that hSGLT1 is expressed in the heart capillaries, the described experiments performed with muscle strips in glucose-containing media are not well suited to determine the role of glucose delivery in the heart. Perfused heart preparations of rat could be used to estimate the role of SGLT1 for glucose delivery in health and disease.

Acknowledgments The authors acknowledge the technical help by Mrs. Eva Heršak. This work was supported by the grant 022-0222148-2146 from Croatian Ministry for Science, Education and Sports (I.S.) and by Deutsche Forschungsgemeinschaft Grant KO 872/5-1 (H.K.).

References

1. Abdul-Ghani MA, DeFronzo RA, Norton L (2013) Novel hypothesis to explain why SGLT2 inhibitors inhibit only 30-50 % of filtered glucose load in humans. Diabetes 62:3324–3328
2. Balen D, Ljubojevic M, Breljak D, Brzica H, Zlender V, Koepsell H, Sabolic I (2008) Revised immunolocalization of the Na^+-D-glucose cotransporter SGLT1 in rat organs with an improved antibody. Am J Physiol Cell Physiol 295:C475–C489
3. Banerjee SK, McGaffin KR, Pastor-Soler NM, Ahmad F (2009) SGLT1 is a novel cardiac glucose transporter that is perturbed in disease states. Cardiovasc Res 84:111–118
4. Basset G, Crone C, Saumon G (1987) Fluid absorption by rat lung in situ: pathways for sodium entry in the luminal membrane of alveolar epithelium. J Physiol 384:325–345
5. Basset G, Saumon G, Bouchonnet F, Crone C (1988) Apical sodium-sugar transport in pulmonary epithelium in situ. Biochim Biophys Acta 942:11–18
6. Bodega F, Sironi C, Armilli M, Porta C, Agostoni E (2010) Evidence for Na^+-glucose cotransporter in type I alveolar epithelium. Histochem Cell Biol 134:129–136
7. Bradford MM (1976) A rapid and sensitive method for the quantification of microgram quantities of protein utilizing the principle of protein-dye binding. Anal Biochem 72:248–254
8. Chen J, Williams S, Ho S, Loraine H, Hagan D, Whaley JM, Feder JN (2010) Quantitative PCR tissue expression profiling of the human SGLT2 gene and related family members. Diabetes Ther 1:57–92
9. Crafer SM, Pryor JS, Dawson AP (1994) Effect of arterial-portal glucose gradients and phloridzin on bile glucose levels in perfused rat liver. J Physiol 479(Pt 2):281–289
10. Dahlin A, Royall J, Hohmann JG, Wang J (2009) Expression profiling of the solute carrier gene family in the mouse brain. J Pharmacol Exp Ther 329:558–570
11. Devaskar SU, deMello DE (1996) Cell-specific localization of glucose transporter proteins in mammalian lung. J Clin Endocrinol Metab 81:4373–4378
12. Diez-Sampedro A, Hirayama BA, Osswald C, Gorboulev V, Baumgarten K, Volk C, Wright EM, Koepsell H (2003) A glucose sensor hiding in a family of transporters. Proc Natl Acad Sci U S A 100:11753–11758
13. Elfeber K, Köhler A, Lutzenburg M, Osswald C, Galla HJ, Witte OW, Koepsell H (2004) Localization of the Na(+)-D-glucose cotransporter SGLT1 in the blood-brain barrier. Histochem Cell Biol 121:201–207
14. Elfeber K, Stümpel F, Gorboulev V, Mattig S, Deussen A, Kaissling B, Koepsell H (2004) Na^+-D-glucose cotransporter in muscle capillaries increases glucose permeability. Biochem Biophys Res Commun 314:301–305
15. Evans CM, Williams OW, Tuvim MJ, Nigam R, Mixides GP, Blackburn MR, DeMayo FJ, Burns AR, Smith C, Reynolds SD, Stripp BR, Dickey BF (2004) Mucin is produced by clara cells in the proximal airways of antigen-challenged mice. Am J Respir Cell Mol Biol 31:382–394
16. Gorboulev V, Schürmann A, Vallon V, Kipp H, Jaschke A, Klessen D, Friedrich A, Scherneck S, Rieg T, Cunard R, Veyhl-Wichmann M, Srinivasan A, Balen D, Breljak D, Rexhepaj R, Parker HE, Gribble FM, Reimann F, Lang F, Wiese S, Sabolic I, Sendtner M, Koepsell H (2012) Na^+-D-glucose cotransporter SGLT1 is pivotal for intestinal glucose absorption and glucose-dependent incretin secretion. Diabetes 61:187–196
17. Guzelian P, Boyer JL (1974) Glucose reabsorption from bile. Evidence for a biliohepatic circulation. J Clin Invest 53:526–535
18. Haase W, Heitmann K, Friese W, Ollig D, Koepsell H (1990) Characterization and histochemical localization of the rat intestinal Na^+-D-glucose cotransporter by monoclonal antibodies. Eur J Cell Biol 52:297–309
19. Haase W, Koepsell H (1989) Electron microscopic immunohistochemical localization of components of Na^+-cotransporters along the rat nephron. Eur J Cell Biol 48:360–374
20. Johnston CJ, Mango GW, Finkelstein JN, Stripp BR (1997) Altered pulmonary response to hyperoxia in Clara cell secretory protein deficient mice. Am J Respir Cell Mol Biol 17:147–155

21. Joris L, Quinton PM (1989) Evidence for electrogenic Na-glucose cotransport in tracheal epithelium. Pflugers Arch 415:118–120
22. Kanai Y, Lee W-S, You G, Brown D, Hediger MA (1994) The human kidney low affinity Na^+/glucose cotransporter SGLT2. Delineation of the major renal reabsorptive mechanism for D-glucose. J Clin Invest 93:397–404
23. Kemp PJ, Boyd CAR (1992) Pathways for glucose transport in type II pneumocytes freshly isolated from adult guinea pig lung. Am J Physiol Lung Cell Mol Physiol 263:L612–L616
24. Kipp H, Khoursandi S, Scharlau D, Kinne RKH (2003) More than apical: distribution of SGLT1 in Caco-2 cells. Am J Physiol Cell Physiol 285:C737–C749
25. Lazaridis KN, Pham L, Vroman B, de Groen PC, LaRusso NF (1997) Kinetic and molecular identification of sodium-dependent glucose transporter in normal rat cholangiocytes. Am J Physiol Gastrointest Liver Physiol 272:G1168–G1174
26. Lee W-S, Kanai Y, Wells RG, Hediger MA (1994) The high affinity Na^+/glucose cotransporter. Re-evaluation of function and distribution of expression. J Biol Chem 269:12032–12039
27. Liakos A, Karagianis T, Athanasiadou E, Satigianni M, Mainou M, Paptheodorou K, Bekiari E, Tsapas A (2014) Efficacy and safety of empagliflozin for type 2 diabetes: a systematic review and meta-analysis. Diabetes Obes Metab 16:984–993
28. Liu JJ, Lee T, DeFronzo RA (2012) Why do SGLT2 inhibitors inhibit only 30–50 % of renal glucose reabsorption in humans? Diabetes 61: 2199–2204
29. Macha S, Mattheus M, Halabi A, Pinnetti S, Woerle HJ, Broedl UC (2014) Pharmacokinetics, pharmacodynamics and safety of empagliflozin, a sodium glucose cotransporter 2 (SGLT2) inhibitor, in subjects with renal impairment. Diabetes Obes Metab 16:215–222
30. Mamchaoui K, Makhloufi Y, Saumon G (2002) Glucose transporter gene expression in freshly isolated and cultured rat pneumocytes. Acta Physiol Scand 175:19–24
31. Masyuk AI, Masyuk TV, Tietz PS, Splinter PL, LaRusso NF (2002) Intrahepatic bile ducts transport water in response to absorbed glucose. Am J Physiol Cell Physiol 283:C785–C791
32. Neumiller JJ (2014) Empagliflozin: a new sodium-glucose co-transporter 2 (SGLT2) inhibitor for the treatment of type 2 diabetes. Drugs Context 3:212262, ISSN 1740-4398
33. Parker HE, Adriaenssens A, Rogers G, Richards P, Koepsell H, Reimann F, Gribble FM (2012) Predominant role of active versus facilitative glucose transport for glucagon-like peptide-1 secretion. Diabetologia 55:2445–2455
34. Parker HE, Habib AM, Rogers GJ, Gribble FM, Reimann F (2009) Nutrient-dependent secretion of glucose-dependent insulinotropic polypeptide from primary murine K cells. Diabetologia 52:289–298
35. Pezzulo AA, Gutierrez J, Duschner KS, McConnell KS, Taft PJ, Ernst SE, Yahr TL, Rahmouni K, Klesney-Tait J, Stoltz DA, Zabner J (2011) Glucose depletion in the airway surface liquid is essential for sterility of the airways. PLoS ONE 6:e16166
36. Poppe R, Karbach U, Gambaryan S, Wiesinger H, Lutzenburg M, Kraemer M, Witte OW, Koepsell H (1997) Expression of the Na^+-D-glucose cotransporter SGLT1 in neurons. J Neurochem 69:84–94
37. Powell DR, Smith M, Greer J, Harris A, Zhao S, DaCosta C, Mseeh F, Shadoan MK, Sands A, Zambrowicz B, Ding ZM (2013) LX4211 increases serum glucagon-like peptide 1 and peptide YY levels by reducing sodium/glucose cotransporter 1 (SGLT1)-mediated absorption of intestinal glucose. J Pharmacol Exp Ther 345:250–259
38. Reimann F, Habib AM, Tolhurst G, Parker HE, Rogers GJ, Gribble FM (2008) Glucose sensing in L cells: a primary cell study. Cell Metab 8:532–539
39. Reynolds SD, Malkinson AM (2010) Clara cell: progenitor for the bronchiolar epithelium. Int J Biochem Cell Biol 42:1–4
40. Rutkovskiy A, Bliksoen M, Hillestad V, Amin M, Czibik G, Valen G, Vaage J, Amiry-Moghaddam M, Stenslokken KO (2013) Aquaporin-1 in cardiac endothelial cells is downregulated in ischemia, hypoxia and cardioplegia. J Mol Cell Cardiol 56:22–33
41. Rutkovskiy A, Valen G, Vaage J (2013) Cardiac aquaporins. Basic Res Cardiol 108:393
42. Sabolic I, Skarica M, Gorboulev V, Ljubojevic M, Balen D, Herak-Kramberger CM, Koepsell H (2006) Rat renal glucose transporter SGLT1 exhibits zonal distribution and androgen-dependent gender differences. Am J Physiol Ren Physiol 290:F913–F926
43. Sabolic I, Valenti G, Verbavatz J-M, Van Hoek AN, Verkman AS, Ausiello DA, Brown D (1992) Localization of the CHIP28 water channel in rat kidney. Am J Physiol 263(Cell Physiol 32):C1225–C1233
44. Sabolic I, Vrhovac I, Eror DB, Gerasimova M, Rose M, Breljak D, Ljubojevic M, Brzica H, Sebastiani A, Thal SC, Sauvant C, Kipp H, Vallon V, Koepsell H (2012) Expression of Na^+-D-glucose cotransporter SGLT2 in rodents is kidney-specific and exhibits sex and species differences. Am J Physiol Cell Physiol 302:C1174–C1188
45. Shibazaki T, Tomae M, Ishikawa-Takemura Y, Fushimi N, Itoh F, Yamada M, Isaji M (2012) KGA-2727, a novel selective inhibitor of a high-affinity sodium glucose cotransporter (SGLT1), exhibits antidiabetic efficacy in rodent Models. J Pharmacol Exp Ther 342:288–296
46. Singh G, Katyal SL (1997) Clara cells and Clara cell 10 kD protein (CC10). Am J Respir Cell Mol Biol 17:141–143
47. Stripp BR, Reynolds SD (2008) Maintenance and repair of the bronchiolar epithelium. Proc Am Thorac Soc 5:328–333
48. Takata K, Kasahara T, Kasahara M, Ezaki O, Hirano H (1992) Immunohistochemical localization of Na^+-dependent glucose transporter in rat jejunum. Cell Tissue Res 267:3–9
49. Thenappan T, Goel A, Marsboom G, Fang YH, Toth PT, Zhang HJ, Kajimoto H, Hong Z, Paul J, Wietholt C, Pogoriler J, Piao L, Rehman J, Archer SL (2011) A central role for CD68(+) macrophages in hepatopulmonary syndrome. Reversal by macrophage depletion. Am J Respir Crit Care Med 183:1080–1091
50. Thomson SC, Rieg T, Miracle C, Mansoury H, Whaley J, Vallon V, Singh P (2012) Acute and chronic effects of SGLT2 blockage on glomerular and tubular function in the early diabetic rat. Am J Physiol Regul Integr Comp Physiol 302:R75–R83
51. Uldry M, Thorens B (2004) The SLC2 family of facilitated hexose and polyol transporters. Pflugers Arch-Eur J Physiol 447(5):480–489
52. Vallon V, Gerasimova M, Rose MA, Masuda T, Satriano J, Mayoux E, Koepsell H, Thomson SC, Rieg T (2014) SGLT2 inhibitor empagliflozin reduces renal growth and albuminuria in proportion to hyperglycemia and prevents glomerular hyperfiltration in diabetic Akita mice. Am J Physiol Ren Physiol 306:F194–F204
53. Vallon V, Platt KA, Cunard R, Schroth J, Whaley J, Thomson SC, Koepsell H, Rieg T (2010) SGLT2 mediates glucose reabsorption in the early proximal tubule. J Am Soc Nephrol 22:104–112
54. Veyhl M, Keller T, Gorboulev V, Vernaleken A, Koepsell H (2006) RS1(RSC1A1) regulates the exocytotic pathway of Na^+-D-glucose cotransporter SGLT1. Am J Physiol Ren Physiol 291:F1213–F1223
55. von Lewinski D, Rainer PP, Gasser R, Huber M-S, Khafaga M, Wilhelm B, Haas T, Mächler H, Rössl U, Pieske B (2010) Glucose-transporter-mediated positive inotropic effects in human myocardium of diabetic and nondiabetic patients. Metabolism 59:1020–1028
56. Wright EM, Loo DDF, Hirayama BA (2011) Biology of human sodium glucose transporters. Physiol Rev 91:733–794
57. Yu AS, Hirayama BA, Timbol G, Liu J, Diez-Sampedro A, Kepe V, Satyamurthy N, Huang SC, Wright EM, Barrio JR (2013) Regional distribution of SGLT activity in rat brain in vivo. Am J Physiol Cell Physiol 304:C240–C247

58. Zambrowicz B, Freiman J, Brown PM, Frazier KS, Turnage A, Bronner J, Ruff D, Shadoan M, Banks P, Mseeh F, Rawlins DB, Goodwin NC, Mabon R, Harrison BA, Wilson A, Sands A, Powell DR (2012) LX4211, a dual SGLT1/SGLT2 inhibitor, improved glycemic control in patients with type 2 diabetes in a randomized, placebo-controlled trial. Clin Pharmacol Ther 92: 158–169

59. Zhou L, Cryan EV, D'Andrea MR, Belkowski S, Conway BR, Demarest KT (2003) Human cardiomyocytes express high level of Na^+/glucose cotransporter 1 (SGLT1). J Cell Biochem 90:339–346